



Influence of Variable Properties on Quadratic Convective Flow of Casson Nanofluid Past an Inclined Plane

T. L. Oyekunle¹, M T. Akolade², J. U. Abubakar³, O. T. Olotu⁴
tloyekunle95@gmail.com¹, akolademojeed@yahoo.com², abubakar.ju@unilorin.edu.ng³,
thomasolotu@gmail.com⁴

^{1,2,3,4} Department of Mathematics, Faculty of Physical Sciences, University of Ilorin, Ilorin, Nigeria

Abstract

In this study, the combined effects of thermophysical fluid properties alongside nonlinear thermal and solutal convective processes in an inclined flow region containing Casson nanofluid subjected to slip and convective boundary conditions are considered. Application of induced non-uniform magnetic field strength applied perpendicular to the flow plane and the buoyancy influences are believed responsible for the quadratic convection rate. The prime PDEs are renewed to systems of ODEs via applicable transformations and similarity variables. Assuming a series trial solution, the flow distribution results were obtained numerically by collocation approach with Legendary polynomial basis function. Validation of the numerical results plays favorably when compared with the weighted residual method (Galerkin) and the existing literature. The results reveal that; Casson fluid exhibit a solid characteristic when yield stress is more than the shear stress, pronouncement of nonlinear solutal and thermal buoyancy effects predicts the acceleration of the flow fields greatly compared to the linear model, adherence between the fluid particles and flow surface displayed retardation in shear force thus enhanced the motion of Casson fluid and diminished the energy fields, surface suspension suppresses the flow but energizes both temperature and nanoparticle volume fraction profiles.

Keywords: Thermophysical fluid properties, Quadratic convection, Legendary Polynomial, Casson nanofluid, Inclined Plane, Collocation method.

1. Introduction

The analysis of heat and mass transportation is very demanding due to its applications in the field of sciences, engineering, and industries when operating at high temperatures. Some of these industrial applications include; combustion, electronics cooling, reactor safety, thermal system, drying surfaces, and solar collector, which demonstrate the nonlinearity phenomenon in temperature. The nonlinearity term is considered in the buoyant force due to the heat transfer properties of the fluid and the notable physical significance of the fluid flow (Patil & Kulkarni, 2019).

Applications of quadratic temperature and density variations have motivated some researchers like Jha & Saki, (2019) who analyzed the effects of the chemical reaction and diffusion thermo on convective heat and mass transfer under nonlinear Boussinesq approximations through a vertical moving plate. It is noticed that higher values of nonlinear convection enhance the velocity profile. The effects of roughness (slip) on MHD nonlinear mixed convection flow of nano liquid through a vertical moving plate is investigated by Patil & Kulkarni, (2019). Raju, et al. (2017) examined nonlinear convection in

Casson fluid flow with time dependency in a porous medium over a rotating cone while Raju, et al. (2018) analyzed the nonlinear convection of an unsteady Casson fluid through a rotating cone with Darcy porous medium. They discovered that an increase in nonlinear thermal and solutal convection parameters leads to more friction force between the particle in the two directions. Kumar & Sood, (2016) examined the combined effects of magnetic field and nonlinear convection on two-dimensional boundary layer stagnation point flow due to shrinking sheet. They observed that both magnetic field and nonlinear convection parameters enhance the solution range significantly. Hayat, et al. (2018) studied the effects of quadratic mixed convection flow taking thermophoresis and Brownian movement into consideration. Recently, Akolade, et al. (2021a) and Idowu, et al. (2021) investigated the nonlinear thermal and solutal convection impact on the magnetized motion of Casson fluid, the first on variable slendering sheet and the latter through an annular medium. They concluded that the temperature and velocity increase with quadratic convection parameter while a decrease is observed in the concentration fields. Other researchers who have considered the solutal and thermal convection in the quadratic form include; Upadhya, et al. (2018a), (2018b),

Kumar, et al. (2017), Ibrahim, et al. (2017), Nagaendramma, et al. (2018) among others.

The thermal conductivity and viscosity are very sensitive to temperature rises, which usually causes significant changes in the physical properties of the fluid, most especially in the theory of lubrication where they are been affected by the heat generated by internal friction and a corresponding temperature rise (Akolade, et al. (2021b), and Jawali & Chamkha, (2015)). The fluctuation of viscosity resulting from variations of temperature or species composition is applicable in engineering and environmental when encountered turbulent flows. The temperature rises with the local transport phenomena by reducing the viscosity across the momentum boundary layer and affected greatly the heat transport rate at the wall.

These applications lead Jawali & Chamkha (2015) to investigate the variable properties on the free convective flow of a viscous fluid in a vertical channel. It is found that the velocity and temperature increase with variable viscosity parameters. Hayat, et al. (2016) examined the variable conductivity and viscosity with unsteadiness in the mixed convective flow. The effect of variable properties on Casson nanofluid flow with convective heating and velocity slip is examined by Gbadeyan, et al. (2020). The results show that the velocity increases with variable properties while a decrease is observed in nanoparticle volume fraction and temperature. The dissipative viscous fluid flow through a spinning cone with mixed convection and variable properties is investigated by Malik, et al. (2016). Salawu and Dada, (2016) analyzed the radioactive temperature change of variable conductivity and viscosity in a non-Darcian medium with inclined magnetic field and dissipation. The use of viscous fluid flow and mixed convection in a vertical channel is carried out by Umavathi, et al. (2017). Other research works on variable properties with various physical effects and geometries includes; Idowu, et al. (2020), Animasaun, (2015), Kench, et al. (2017), Kumar, et al. (2017), Akolade, et al. (2021a) to mention but a few.

Casson fluid is one of the types of non-Newtonian fluids which behave like an elastic solid, it has a shear-thinning liquid and assumed stress below which no flow occurs and a zero viscosity at an infinite rate of shear. It is found useful in engineering and industries like coating and polymer processing, paper production, aerodynamic heating, and petroleum (Animasaun, 2015). Its applications in many processes occurring in nature and industries attracted the attention of some researchers such as Kala, et al. (2020) who analyzed the flow of Casson fluid in a magnetic field with velocity slip in a Forchheimer porous medium through an inclined nonlinearly stretching surface. The result shows that the velocity boundary layer thickness and the absolute value of velocity reduce with a hike in the Casson number while the reverse is the case for thermal boundary layer thickness and an absolute value of temperature. Analysis of MHD Casson fluid flow through a permeable stretching sheet with heat and mass transfer is investigated by Asogwa, et al. (2020). Investigation of Casson fluid in squeezing motion with variable thermophysical features by Akolade, et al. (2021b) reveals that more injection of

Casson number downsized the velocities and energy fields. Generalized heat flux in Casson fluid over a slendering surface is discussed in Akolade, et al. (2021a), and Idowu, et al. (2020).

To the author's best knowledge, the combined investigation of variable properties influence on quadratic convection flow of Casson Nanofluid past an inclined plane with slip condition is still far-fetched in the literature, which is the aim of the study. The governing equations of the flow are nondimensionalized and transformed to a set of coupled nonlinear ordinary differential equations. Collocation method with assumed Legendary polynomial basis trial function and MATHEMATICAL 11.0 software is employed to achieve approximate solutions of the flow distributions and characteristics.

2. Model formulation

An incompressible, laminar, electrically conducting, and steady flow with quadratic convective motion of Casson nanofluid through porous and inclined plane geometry is investigated. As shown in Figure 1, the flow is assumed two dimensional, \bar{y}_1 -axis taken flow streamwise while \bar{y}_2 -axis is assumed perpendicular to it, with the magnetic field $B(\bar{y}_1) = B_0 \bar{y}_1^{-0.5}$ perpendicular to the flow streamwise, variable electrical field effect $\sigma^* = \sigma_0 \bar{u}_1$ is applied,

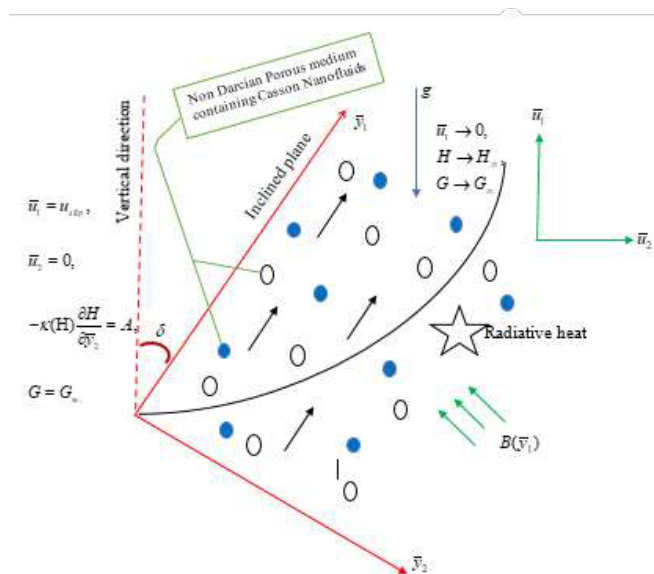


Figure 1: Problem flow geometry of an inclined plane

where σ_0 B_0 is the constant electrical and magnetic field influence respectively is been applied normally to the fluid flow direction. The surface of the plate and free stream temperatures are taken to be H_f and H_∞ accordingly, while the wall and free stream mass transfer are taken to be G_w and G_∞ respectively.

2.1. Governing Equations

Based on the above assumption, boundary layer, and nullifying the usual Boussinesq approximation theory, the Casson nanofluid motion is governed by the following flow model equations (Uddin et al. 2012, Animasaun 2015, Gbadeyan et al. 2020, and Akolade et al 2021b).

$$\frac{\partial \bar{u}_1}{\partial \bar{y}_1} + \frac{\partial \bar{u}_2}{\partial \bar{y}_2} = 0 \quad (1)$$

$$\begin{aligned} \rho_f \left(\bar{u}_1 \frac{\partial \bar{u}_1}{\partial \bar{y}_1} + \bar{u}_2 \frac{\partial \bar{u}_1}{\partial \bar{y}_2} \right) &= \left(1 + \frac{1}{\alpha} \right) \frac{\partial}{\partial \bar{y}_2} \left(\mu(H) \frac{\partial \bar{u}_1}{\partial \bar{y}_2} \right) \\ &- \sigma_0 B^2 (\bar{y}_1) \bar{u}_1^2 - \frac{\mu(H)(1+\alpha^{-1})}{k_p} \bar{u}_1 - \frac{b^*}{k_p} \bar{u}_1^2 + \\ &g \cos(\delta) \left[\lambda_1 (H - H_\infty) + \lambda_1 (H - H_\infty)^2 \right. \\ &\left. + \lambda_3 (G - G_\infty) + \lambda_4 (G - G_\infty)^2 \right] \end{aligned} \quad (2)$$

$$\begin{aligned} \bar{u}_1 \frac{\partial H}{\partial \bar{y}_1} + \bar{u}_2 \frac{\partial H}{\partial \bar{y}_2} &= \tau \left[D_B \frac{\partial G}{\partial \bar{y}_2} \frac{\partial H}{\partial \bar{y}_2} + \frac{D_H}{H_\infty} \left(\frac{\partial H}{\partial \bar{y}_2} \right)^2 \right] + \\ &\frac{1}{\rho_f c_p} \frac{\partial}{\partial \bar{y}_2} \left(\kappa(H) \frac{\partial H}{\partial \bar{y}_2} \right) - \frac{1}{\rho_f c_p} \frac{\partial q_r}{\partial \bar{y}_2} + \\ Q_1 (H - H_\infty) &+ \frac{D_m k_0}{c_s c_p} \frac{\partial^2 G}{\partial \bar{y}_2^2} + \frac{\mu(H)(1+\alpha^{-1})}{\rho_f c_p} \left(\frac{\partial \bar{u}_1}{\partial \bar{y}_2} \right)^2, \end{aligned} \quad (3)$$

$$\begin{aligned} \bar{u}_1 \frac{\partial G}{\partial \bar{y}_1} + \bar{u}_2 \frac{\partial G}{\partial \bar{y}_2} &= \frac{D_m k_0}{H_m} \frac{\partial^2 H}{\partial \bar{y}_2^2} + \\ &\frac{D_H}{H_\infty} \frac{\partial^2 H}{\partial \bar{y}_2^2} + D_B \frac{\partial^2 G}{\partial \bar{y}_2^2} - k^* (G - G_\infty) \end{aligned} \quad (4)$$

With the boundary conditions

$$\begin{cases} \bar{u}_1 = u_{slip}, \bar{u}_2 = 0, -\kappa(H) \frac{\partial H}{\partial \bar{y}_2} = A, G = G_w, \text{ at } \bar{y}_2 = 0, \\ \bar{u}_1 = 0, H \rightarrow H_\infty, G \rightarrow G_\infty \text{ as } \bar{y}_2 \rightarrow \infty. \end{cases} \quad (5)$$

Where

$$A = h_f(\bar{y}_1)(H_f - H), u_{slip} = s_1 \frac{\mu(H)}{\rho_f} \left(1 + \frac{1}{\alpha} \right) \frac{\partial \bar{u}_1}{\partial \bar{y}_2},$$

The diffusion Rossland approximation heat flux is defined (Idowu & Falodun (2020))

$$q_r = \frac{4\sigma_1}{3k_1} \frac{\partial H^4}{\partial \bar{y}_2}, \quad (6)$$

Following Akolade, et al. (2021a) and (2021b) and Idowu & Falodun (2020), the linear form of thermal conductivity and temperature-dependent plastic dynamic viscosity is as thus:

$$\mu(H) = \mu_0 [1 + a_i (H_w - H)], \kappa(H) = \kappa_0 [1 + a_j (H - H_\infty)]. \quad (7)$$

2.2. Dimensionless transformation

To put the governing PDEs systems of Eqns (1) – (5) into dimensionless form and invoking Eqns (6) and (7), we introduced non-dimensional variables (Uddin et al. 2012 and Gbadeyan et al. 2020);

$$u_2 = \frac{\bar{u}_2 L}{\alpha^* Ra^{0.25}}, \omega = \frac{G - G_\infty}{G_w - G_\infty}, \chi = \frac{H - H_\infty}{H_f - H_\infty}. \quad (8)$$

$$y_1 = \frac{\bar{y}_1}{L}, y_2 = \frac{\bar{y}_2 Ra^{0.25}}{L}, u_1 = \frac{\bar{u}_1 L}{\alpha^* Ra^{0.5}}.$$

Hence, the dimensionless form of Eqns (1) – (5) are as thus;

$$\frac{\partial u_1}{\partial y_1} + \frac{\partial u_2}{\partial y_2} = 0 \quad (9)$$

$$\begin{aligned} P_r \left(1 + \frac{1}{\alpha} \right) \left[\left\{ 1 + \gamma_1 (1 - \chi) \right\} \left(\frac{\partial^2 u}{\partial y_2^2} - \frac{L^2}{k_p Ra^{0.5}} u \right) \right] &= \\ u_1 \frac{\partial u_1}{\partial y_1} + u_2 \frac{\partial u_1}{\partial y_2} + P_r \left(1 + \frac{1}{\alpha} \right) \gamma_1 \frac{\partial u_1}{\partial y_2} \frac{\partial \chi}{\partial y_2} &+ \left(\frac{J}{y_1} + \frac{b^* L}{k_p} \right) u_1^2, \quad (10) \\ -P_r \cos \delta \left[\left(\chi + \varepsilon_1 \chi^2 \right) + Nr \left(\omega + \varepsilon_2 \omega^2 \right) \right] \end{aligned}$$

$$\begin{aligned} u_1 \frac{\partial \chi}{\partial y_1} + u_2 \frac{\partial \chi}{\partial y_2} &= \left\{ 1 + \gamma_2 \chi + \frac{4}{3} R \right\} \frac{\partial^2 \chi}{\partial y_2^2} + \\ Nb \frac{\partial \omega}{\partial y_2} \frac{\partial \chi}{\partial y_2} + \{ Nt + \gamma_2 \} \left(\frac{\partial \chi}{\partial y_2} \right)^2 &+ Q_2 \chi + Df \frac{\partial^2 \omega}{\partial y_2^2} +, \quad (11) \\ P_r \frac{\alpha^* Ra}{L^2 C_p (H_f - H_\infty)} \{ 1 + \gamma_1 (1 - \chi) \} \left(1 + \frac{1}{\alpha} \right) &\left(\frac{\partial u_1}{\partial y_2} \right)^2 \end{aligned}$$

$$u_1 \frac{\partial \omega}{\partial y_1} + u_2 \frac{\partial \omega}{\partial y_2} = \left(\frac{Nt}{Nb} \frac{1}{Le} + Sr \right) \frac{\partial^2 \chi}{\partial y_2^2} + \frac{1}{Le} \frac{\partial^2 \omega}{\partial y_2^2} - \gamma \omega, \quad (12)$$

Subjected to the boundary conditions

$$\begin{cases} u_1 = \frac{s_1 Ra^{0.25}}{\rho_f L} \{1 + \gamma_1(1 - \chi)\} \left(1 + \frac{1}{\alpha}\right) \frac{\partial u_1}{\partial y_2}, u_2 = 0, \\ \frac{\partial \chi}{\partial y_2} = -\frac{L h_f(y_1) Bi(1 - \chi)}{k_0 Ra^{0.25} (1 + \gamma_2 \chi)}, \omega = 1 \text{ at } y_2 = 0, \\ u_1 \rightarrow 0, \chi \rightarrow 0, \omega \rightarrow 0, \text{ as } y_2 \rightarrow \infty. \end{cases} \quad (13)$$

Where

$$\begin{aligned} Sr &= \frac{D_m k_0 (H_f - H_\infty)}{T_m \alpha^* (G_w - G_\infty)}, R = \frac{4 \sigma_1 H_\infty^3}{3 k_1 k}, \\ \gamma &= \frac{k^* L^2}{\alpha^* Ra^{0.5}}, Df = \frac{D_m k_0 (G_w - G_\infty)}{\alpha^* C_s C_p (H_f - H_\infty)}, J = \frac{\sigma_0 B_0^2}{\rho_f}, \\ Nt &= \frac{\tau D_t (H_f - H_\infty)}{H_\infty \alpha^*}, Nb = \frac{\tau D_B (G_w - G_\infty)}{\alpha^*}, Le = \frac{\alpha^*}{D_B}, \\ Pr &= \frac{\nu}{\alpha^*}, Nr = \frac{\lambda_3 (G_w - G_\infty)}{\lambda_1 (H_f - H_\infty)}, Q_2 = \frac{L^2 Q_1}{\alpha^* Ra^{0.5} \rho_f C_p}, \\ \gamma_1 &= a_i (H_f - H_\infty), \gamma_2 = a_j (H_f - H_\infty), \\ \varepsilon_1 &= \frac{\lambda_2}{\lambda_1} (H_f - H_\infty), \varepsilon_2 = \frac{\lambda_4}{\lambda_3} (G_w - G_\infty), \\ Q_2 &= \frac{L^2 Q_1}{\alpha^* Ra^{0.5} \rho_f c_p} Ra = \frac{(H_f - H_\infty) \lambda_1 g L^3}{\alpha^* \nu} \end{aligned}$$

2.3. Stream function transformation

$$\text{With the stream function } u_1 = \frac{\partial \psi}{\partial y_2}, u_2 = -\frac{\partial \psi}{\partial y_1}, \text{ Eq (9)}$$

is automatically satisfied then Eqs (10) – (13) transformed to;

$$\begin{aligned} P_r \left(1 + \frac{1}{\alpha}\right) \{1 + \gamma_1(1 - \chi)\} \left[\frac{\partial^3 \psi}{\partial y_2^3} - \frac{L^2}{k_p Ra^{0.5}} \frac{\partial \psi}{\partial y_2} \right] &= \\ \frac{\partial \psi}{\partial y_2} \frac{\partial^2 \psi}{\partial y_1 \partial y_2} - \frac{\partial \psi}{\partial y_1} \frac{\partial^2 \psi}{\partial y_2^2} + \left\{ \frac{J}{x} + \frac{b^* L}{k_p} \right\} \left(\frac{\partial \psi}{\partial y_2} \right)^2 &+ \quad (14) \\ P_r \left(1 + \frac{1}{\alpha}\right) \gamma_1 \frac{\partial \chi}{\partial y_2} \frac{\partial^2 \psi}{\partial y_2^2} - P_r \cos \delta \left[\frac{(\chi + \varepsilon_1 \chi^2) +}{Nr(\omega + \varepsilon_2 \omega^2)} \right] & \end{aligned}$$

$$\begin{aligned} \frac{\partial \psi}{\partial y_2} \frac{\partial \chi}{\partial y_1} - \frac{\partial \psi}{\partial y_1} \frac{\partial \chi}{\partial y_2} &= \left\{ 1 + \gamma_2 \chi + \frac{4}{3} R \right\} \frac{\partial^2 \chi}{\partial y_2^2} + \\ Nb \frac{\partial \omega}{\partial y_2} \frac{\partial \chi}{\partial y_2} + \{Nt + \gamma_2\} \left(\frac{\partial \chi}{\partial y_2} \right)^2 &+ Q_2 \chi + Df \frac{\partial^2 \omega}{\partial y_2^2} + \quad (15) \end{aligned}$$

$$P_r \frac{\alpha^* Ra}{L^2 C_p (H_f - H_\infty)} \{1 + \gamma_1(1 - \chi)\} \left(1 + \frac{1}{\alpha}\right) \left(\frac{\partial^2 \psi}{\partial y_2^2} \right)^2,$$

$$\frac{\partial \psi}{\partial y_2} \frac{\partial \omega}{\partial y_1} - \frac{\partial \psi}{\partial y_1} \frac{\partial \omega}{\partial y_2} = \frac{1}{Le} \frac{\partial^2 \omega}{\partial y_2^2} + \left(\frac{Nt}{Nb Le} + Sr \right) \frac{\partial^2 \chi}{\partial y_2^2} - \gamma \omega, \quad (16)$$

with boundary conditions

$$\begin{cases} \frac{\partial \psi}{\partial y_2} = \frac{s_1 Ra^{0.25}}{\rho_f L} \{1 + \gamma_1(1 - \chi)\} \left(1 + \frac{1}{\alpha}\right) \left(\frac{\partial^2 \psi}{\partial y_2^2} \right), \\ \frac{\partial \chi}{\partial y_2} = -\frac{L h_f(y_1) (1 - \chi)}{k_0 Ra^{0.25} (1 + \gamma_2 \chi)}, \phi = 1, \text{ at } y = 0, \\ \frac{\partial \psi}{\partial y} \rightarrow 0, \theta \rightarrow 0, \phi \rightarrow 0, \text{ as } y \rightarrow \infty. \end{cases} \quad (17)$$

2.4. Similarity transformation

The following similarity variables are used (Uddin et al. 2012 and Gbadeyan et al. 2020);

$$\tau = \frac{y_2}{y_1^{0.25}}, \psi = y_1^{0.75} h(\tau), \chi = \chi(\tau), \quad (18)$$

$$k_p = y_1^{0.5} (k_p)_0, h_f(y_1) = y_1^{0.25} (h_f)_0, b^* = y_1^{-0.5} (b^*)_0$$

Implementing the transformations in Eq (18) on the modified systems of Eqs (14) to (17) we have;

$$\begin{aligned} \left(1 + \frac{1}{\alpha}\right) [1 + \gamma_1(1 - \chi)] h''' - \gamma_1 h'' \chi' &+ \\ \frac{1}{4 P_r} [3 h h'' - 2 h'^2 - 4(J + B) h'^2] &+ \\ \cos[\delta] \{(\chi + \varepsilon_1 \chi^2) + N_r(\omega + \varepsilon_2 \omega^2)\} - & \\ \frac{1}{D_a} \left(1 + \frac{1}{\alpha}\right) [1 + \gamma_1(1 - \chi)] h' &= 0 \quad (19) \end{aligned}$$

$$\begin{aligned} (1 + \gamma_2 \chi + \frac{4}{3} R) \chi'' + \frac{3}{4} h \chi' + Nb \omega' \chi' + (\gamma_2 + Nt) \chi'^2 &+ \\ + Q_2 \chi + Df \omega'' + P_r Ec \left(1 + \frac{1}{\alpha}\right) [1 + \gamma_1(1 - \chi)] h'^2 &= 0 \quad (20) \end{aligned}$$

$$\omega'' + \frac{3}{4} Le h \omega' - Le \gamma \omega + \left(\frac{Nt}{Nb} + Le S_r \right) \chi'' = 0, \quad (21)$$

With boundary conditions

$$\begin{aligned} h'(0) &= s_2[1 + \gamma_1(1 - \chi)]\left(1 + \frac{1}{\alpha}\right)h''(0), \\ h(0) &= 0, \quad \chi'(0) = -\frac{B_1(1-\chi(0))}{(1+\gamma_2\chi)}, \quad \omega(0) = 1, \\ h'(\infty) &\rightarrow 0, \quad \chi(\infty) \rightarrow 0, \quad \omega(\infty) \rightarrow 0. \end{aligned} \quad (22)$$

where

$$Ec = \frac{\alpha^2 Ra}{L^2 c_p (H_f - H_\infty)}, Da = \frac{(k_p)_0 Ra^{\frac{1}{2}}}{L^2}, B = \frac{(b^*)_0 L}{(k_p)_0}, Bi = \frac{(h_f)_0 L}{k Ra^{\frac{1}{4}}}, s_2 = \frac{s_1 \mu_0 Ra^{0.25}}{\rho_f L}$$

2.5. Engineering Physical characteristics

Following Uddin et al (2012) and Gbadeyan et al. (2020), the flow characteristics are defined as;

$$Nu_{\bar{y}_1} = -\bar{y}_1 \left(\frac{\partial H}{\partial \bar{y}_2} \right)_{\bar{y}_2=0}, \text{ and } Sh_{\bar{y}_1} = -\bar{y}_1 \left(\frac{\partial G}{\partial \bar{y}_2} \right)_{\bar{y}_2=0}. \quad (23)$$

Implementing the stream function ψ along with Eqs (8) and (18) on Eq (23) results to the reduced Nusselt and Sherwood numbers respectively;

$$Ra_{\bar{y}_1}^{-0.25} Nu_{\bar{y}_1} = -\chi'(0), \text{ and } Ra_{\bar{y}_1}^{-0.25} Sh_{\bar{y}_1} = -\omega'(0), \quad (24)$$

3. Numerical procedure

The solutions to the non-linear, coupled, ODEs in Eqs (19)–(22) are obtained via collocation technique with Legendre polynomial as the basis function. The problem boundary is $[0, \infty)$, to implement this numerical method, the domain is first truncated using the domain truncation approach $[0, L]$. The Legendre polynomial defined on $[-1, 1]$ is transformed to $[0, L]$ via algebraic mapping,

$$\xi = \frac{2\tau}{L} - 1, \quad \xi \in [-1, +1]. \quad (28)$$

The unknown function $h(\tau)$, $\chi(\tau)$, and $\omega(\tau)$ are approximated by the sum of a finite series of the legendary polynomial (Z_j) as

$$\begin{aligned} h(\tau) &\approx h_N(\xi) = \sum_{j=0}^N a_j \left(\frac{2\tau}{L} - 1 \right) Z_j, \\ \chi(\tau) &\approx \chi_N(\xi) = \sum_{j=0}^N b_j \left(\frac{2\tau}{L} - 1 \right) Z_j, \text{ for } j=0,1,\dots,N, \\ \omega(\tau) &\approx \omega_N(\xi) = \sum_{j=0}^N c_j \left(\frac{2\tau}{L} - 1 \right) Z_j, \end{aligned} \quad (29)$$

$h(\xi)$, $\chi(\xi)$ and $\omega(\xi)$ are approximate series of $h(\tau)$, $\chi(\tau)$ and $\omega(\tau)$ respectively at N collocation points, and a_j , b_j and c_j are the unknown constants to be

determined.

The generated equations of $3N+3$ algebraic systems with $3N+3$ unknown coefficient is solved via a MATHEMATICA 11.0 symbolic package with newton iteration technique to simulate the system of derived algebraic equations to obtain the required constants coefficients (a_j , b_j and c_j). Hence, solutions are obtained for the flow distributions and characteristics.

4. Results and Discussion

The coupled non-linear ordinary differential equations (19) – (21) with boundary condition (22) are solved. The results show the influence of different pertinent parameters involved on the velocity, energy, and nanoparticle volume fractions distributions along with the engineering flow characteristics. Following Gbadeyan, et al. (2020) and Uddin, et al. (2012), the default values employed in this study are $\gamma_1 = \gamma_2 = 0.3$, $P_r = 0.71$, $Nt = B = 0.1$,

$$R = Nb = 0.1, \quad \varepsilon_1 = \varepsilon_2 = 1.5, \quad Nr = 1, \quad Ec = 0.01, \\ s_2 = 0.3, \quad \delta = \frac{\pi}{6}, \quad \alpha = 0.3, \quad Df = 0.01, \quad Sr = 0.3, \\ Da = 5, \quad Le = 1, \quad H = Bi = 0.5, \quad G = 0.03, \quad \gamma = 0.2$$

else otherwise stated. The obtained results are compared with the existing works of Uddin et al. (2012) and Gbadeyan, et al. (2020) when the introduced parameters are set to zero and the results are found to give an excellent agreement (see Table 1). Also, a numerical comparison is carried out using Galerkin Weighted Residual method, the results are as shown in Tables 2.

Figures 2 and 3 portray the variable viscosity (γ_1) and thermal conductivity (γ_2) effects on flow distributions. It is observed from Figure 2 that the velocity diminished with a hike in the viscosity parameter while the acceleration is noticed in the energy field. Figure 3 reveals that the velocity and temperature profiles are enhanced with a raise in a thermal variable while reduction is realized in the case of nanoparticle volume fraction. Physically, the fluid thickness (temperature-dependent viscosity) and conductivity are very important and indispensable to foresee the flow behavior suspiciously.

The effects of inclination angle (δ) on velocity, temperature, and concentration distributions are registered in Figure 4. It is shown from the figure that an increase δ reduces the velocity distribution and speeds up the temperature along with the nanoparticle volume fraction profiles. Actually, the impact of larger values of inclination angle is to build a stronger impression on the external magnetic field.

The impact of thermal and solutal convection (ε_1 and ε_2) on the flow field are displayed in Figures 5 and 6 respectively. The result shows that a rise in ε_1 improving the particle interaction nonlinearly, which leads to an

increase in velocity and a reduction in temperature profile (see Figure 5). Figure 6 reveals that an increase in solutal convection causes a slight increase in velocity distribution.

Physically, for the convection process, an upgraded material thermal conductivity is required for a perfect prediction of heat and mass transfer across the flow region.

Table 1: Comparison of Uddin et al. (2012), Gbadeyan et al. (2020), and present results of Nusselt number for $N_t = 0.1, D_a = \alpha \rightarrow \infty, Bi = L_e = 10, \gamma_1 = \gamma_2 = s_2 = \delta = J_1 = J_2 = E_c = R = B = H = \gamma = G = D_f = S_r = 0$,

Values		$P_r = 1.0$			$P_r = 5$		
N_b	$-N_r$	Uddin et al. (2012)	Gbadeyan et al. (2020)	Present Results	Uddin et al. (2012)	Gbadeyan et al (2020)	Present Results
0.1	0	0.34257	0.342575	0.342556	0.38395	0.383959	0.383434
	0.2	0.33659	0.336593	0.336572	0.37734	0.377351	0.376801
	0.4	0.33012	0.330127	0.330101	0.37024	0.370246	0.369664
	0.6	0.32305	-	0.323022	0.36252	-	0.361908
0.3	0	0.29600	0.295999	0.295983	0.33288	0.332884	0.332436
	0.2	0.29178	0.291778	0.291760	0.32821	0.328211	0.327751
	0.4	0.28724	0.287244	0.287219	0.32322	0.323225	0.322746
	0.6	0.28231	-	0.282290	0.31785	-	0.317355

Table 2: Comparison of Galerkin Weighted Residual Method (GWRM) and Legendary polynomial with Collocation Technique (LCT) on Skinfriction, Nusselt number, and Sharewood number with different values of temperature-dependent properties.

Value		GWRM			LCT		
γ_1	γ_2	$h''(0)$	$-\chi'(0)$	$-\omega'(0)$	$h''(0)$	$-\chi'(0)$	$-\omega'(0)$
0.0	0.2	0.286860	0.189756	0.548231	0.286828	0.189755	0.548231
0.1	0.2	0.272991	0.188416	0.546714	0.272957	0.188416	0.546714
0.2	0.2	0.260324	0.187112	0.545286	0.260288	0.187114	0.545286
0.3	0.2	0.248712	0.185847	0.543939	0.248673	0.185846	0.543939
0.4	0.2	0.238031	0.184612	0.542667	0.237989	0.184612	0.542668
0.0	0.5	0.284692	0.170065	0.562080	0.284658	0.170067	0.562082
0.1	0.5	0.270641	0.168811	0.560483	0.270604	0.168811	0.560485
0.2	0.5	0.257829	0.167592	0.558976	0.257790	0.167591	0.558978
0.3	0.5	0.246104	0.166406	0.557552	0.246062	0.166406	0.557554
0.4	0.5	0.235335	0.165253	0.556203	0.235291	0.165253	0.556206

Table 3: Results of pertinent flow parameters on heat transfer $-\chi'(0)$ and mass transfer coefficients $-\omega'(0)$.

values		$-\chi'(0)$	$-\omega'(0)$	values		$-\chi'(0)$	$-\omega'(0)$
γ_1	0.1	0.181241	0.551880	γ_2	0.0	0.202619	0.531367
	0.3	0.178729	0.549049		0.1	0.193759	0.538098
	0.5	0.176348	0.546523		0.3	0.178729	0.549049
ε_1	0.0	0.172433	0.541848	ε_2	0.0	0.163982	0.533292
	1.0	0.176810	0.546753		1.0	0.174201	0.543719
	2.0	0.180507	0.551261		2.0	0.182913	0.554413
S_2	0.1	0.164003	0.532345	Bi	0.1	0.068752	0.555582
	0.3	0.178729	0.549049		0.4	0.161216	0.550450
	0.5	0.184710	0.557188		0.7	0.204973	0.546756
α	0.1	0.153147	0.527879	δ	30 ⁰	0.178729	0.549049
	0.5	0.185641	0.557510		45 ⁰	0.169730	0.539365
	1.0	0.191723	0.566178		60 ⁰	0.153883	0.526675
Nt	0.1	0.178729	0.549049	Nb	0.2	0.171259	0.576402
	0.2	0.181482	0.508538		0.5	0.155078	0.600207
	0.3	0.184069	0.467751		0.7	0.145256	0.609379
Sr	0.1	0.177673	0.557814	Df	0.01	0.178729	0.549049
	0.3	0.178729	0.549049		0.1	0.163958	0.573822

	0.7	0.180845	0.530837		0.5	0.078952	0.734339
--	-----	----------	----------	--	-----	----------	----------

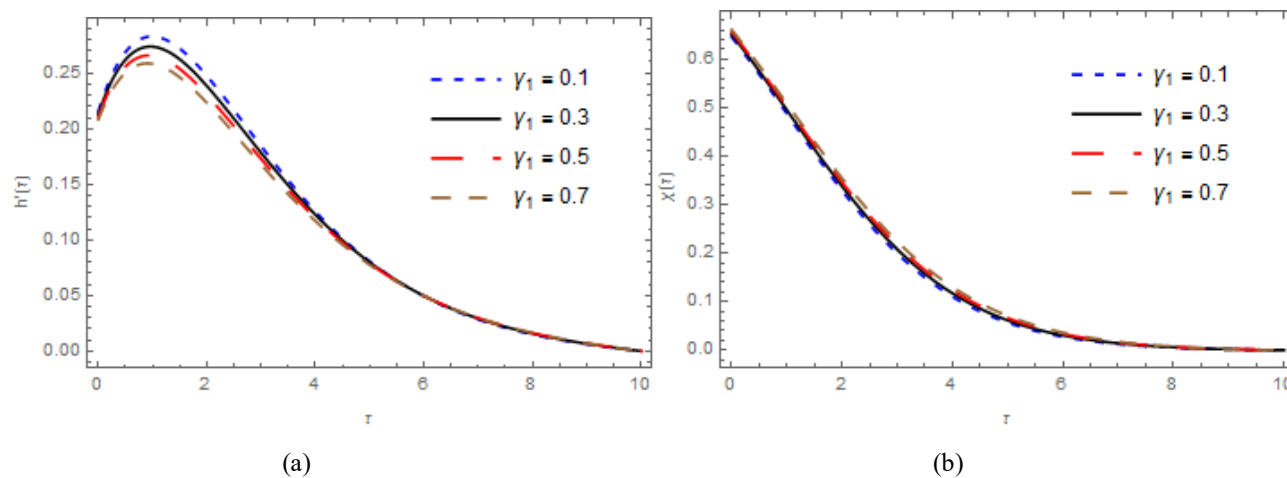


Fig. 2. Variable viscosity (γ_1) impact (a) velocity, and (b) temperature fields

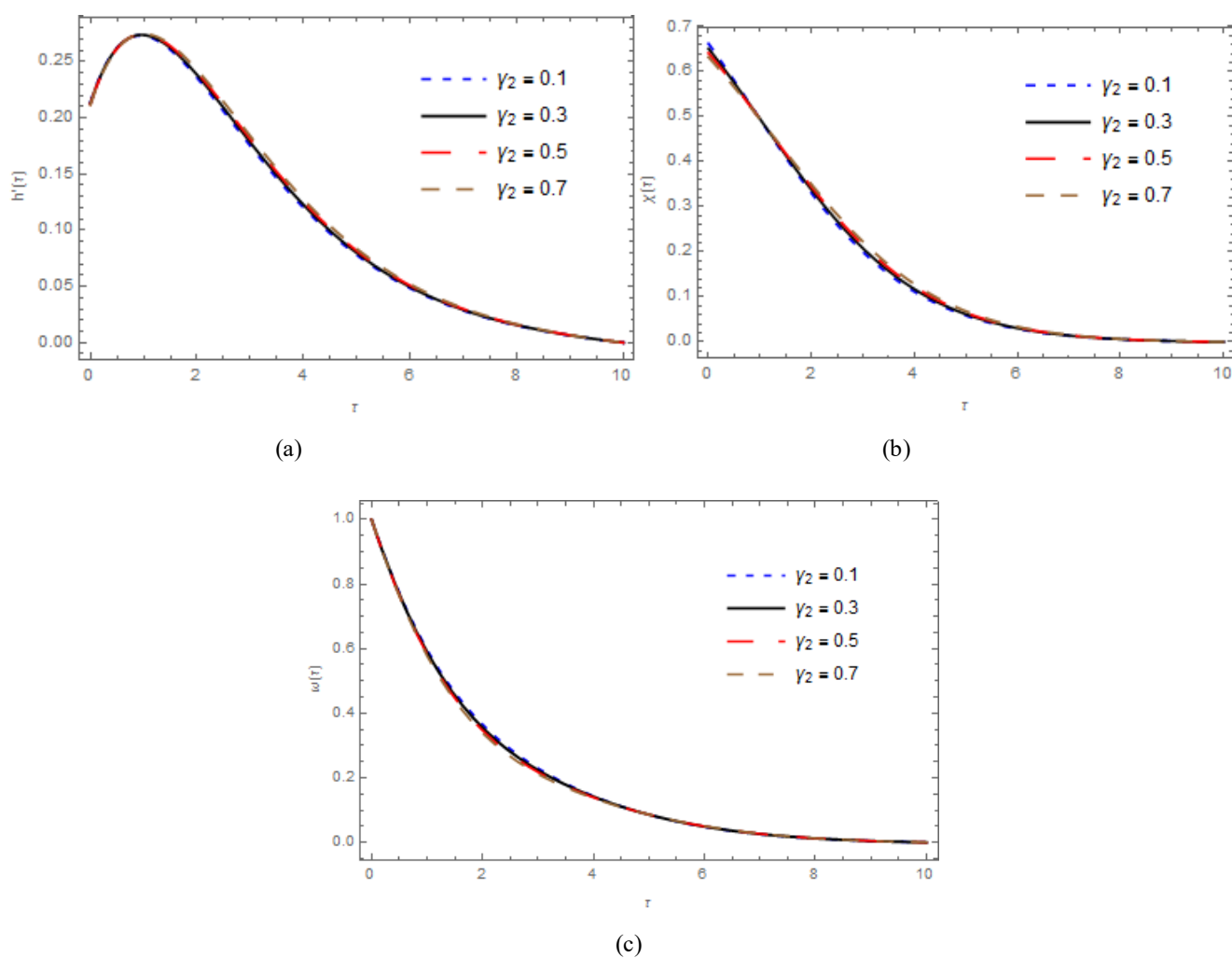


Fig. 3. Variable thermal conductivity (γ_2) impact (a) velocity, (b) temperature, and (c) concentration fields

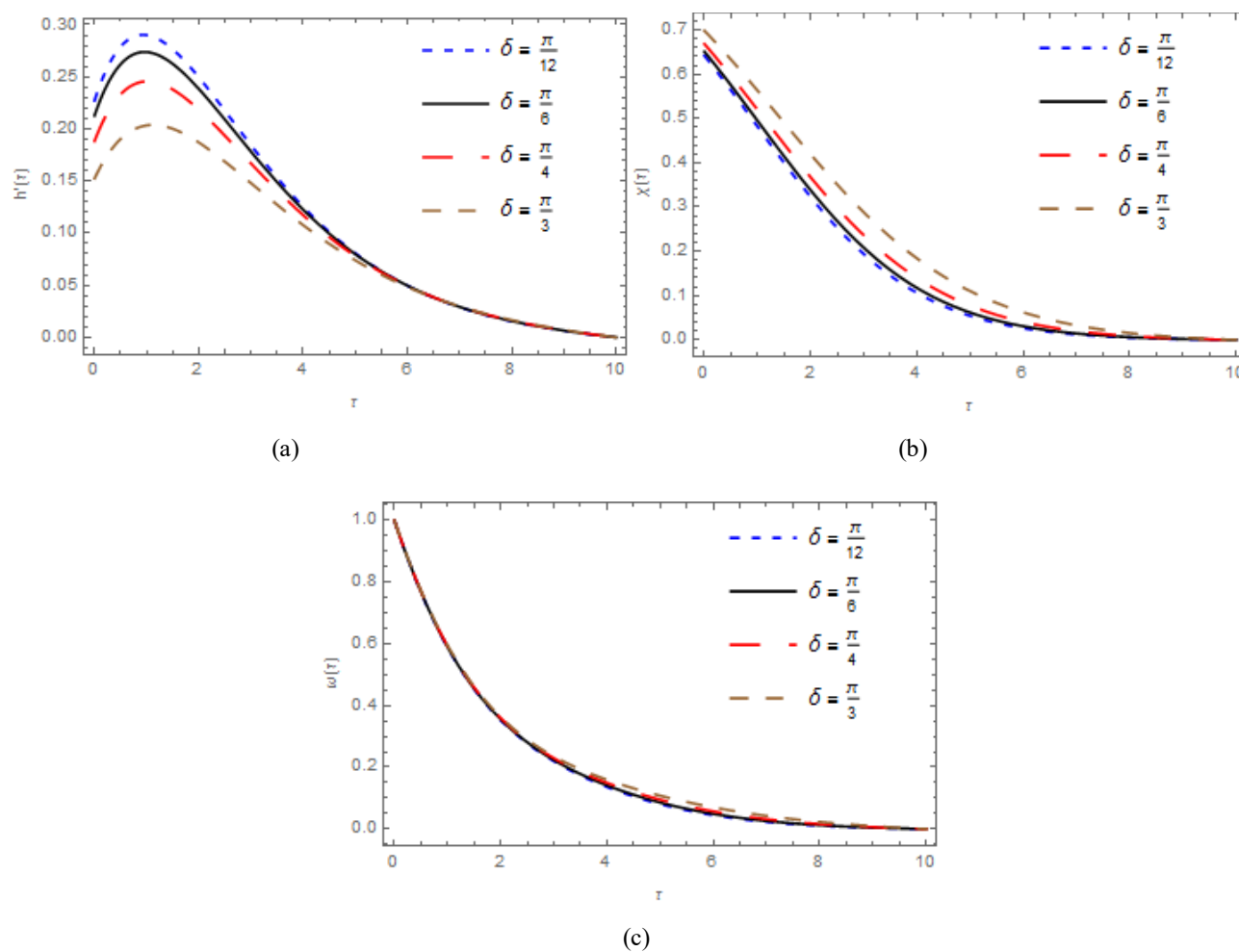


Fig. 4. Inclination (δ) impact on (a) velocity, (b) temperature, and (c) concentration fields

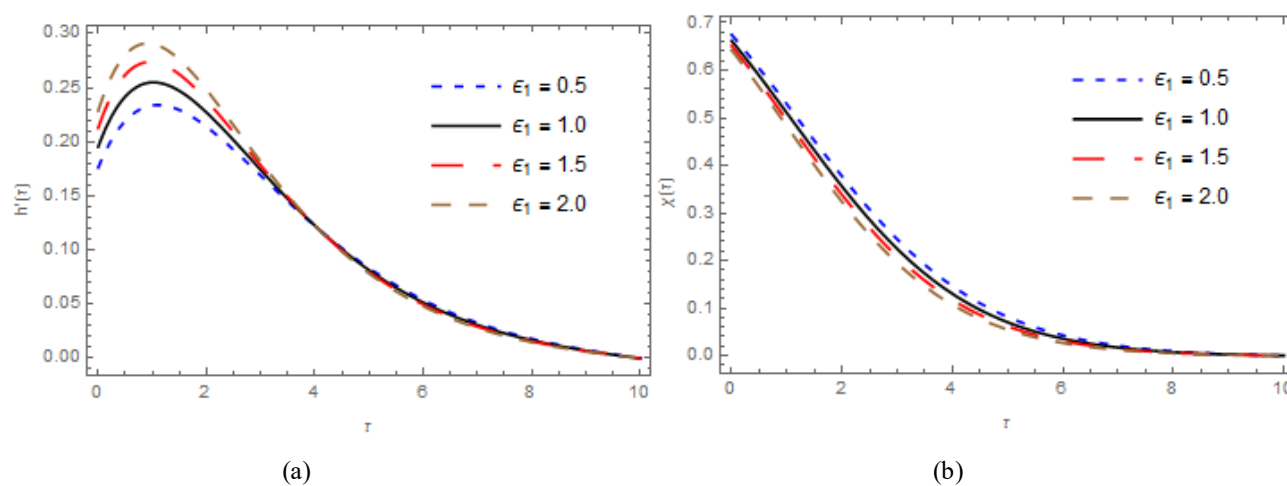


Fig. 5. Nonlinear thermal convection (ϵ_1) impact on (a) velocity and (b) temperature fields

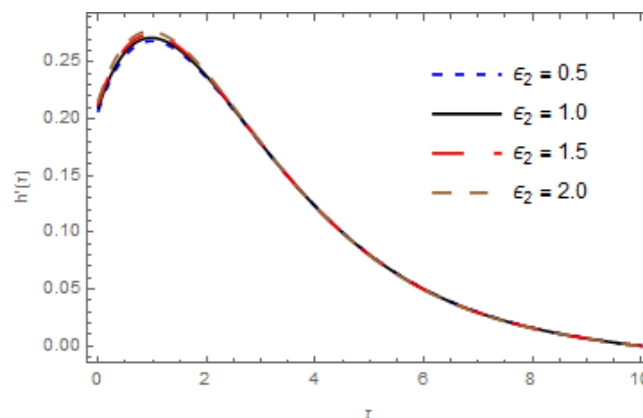


Fig. 6. Nonlinear solutal convection (ϵ_2) impact on the velocity field

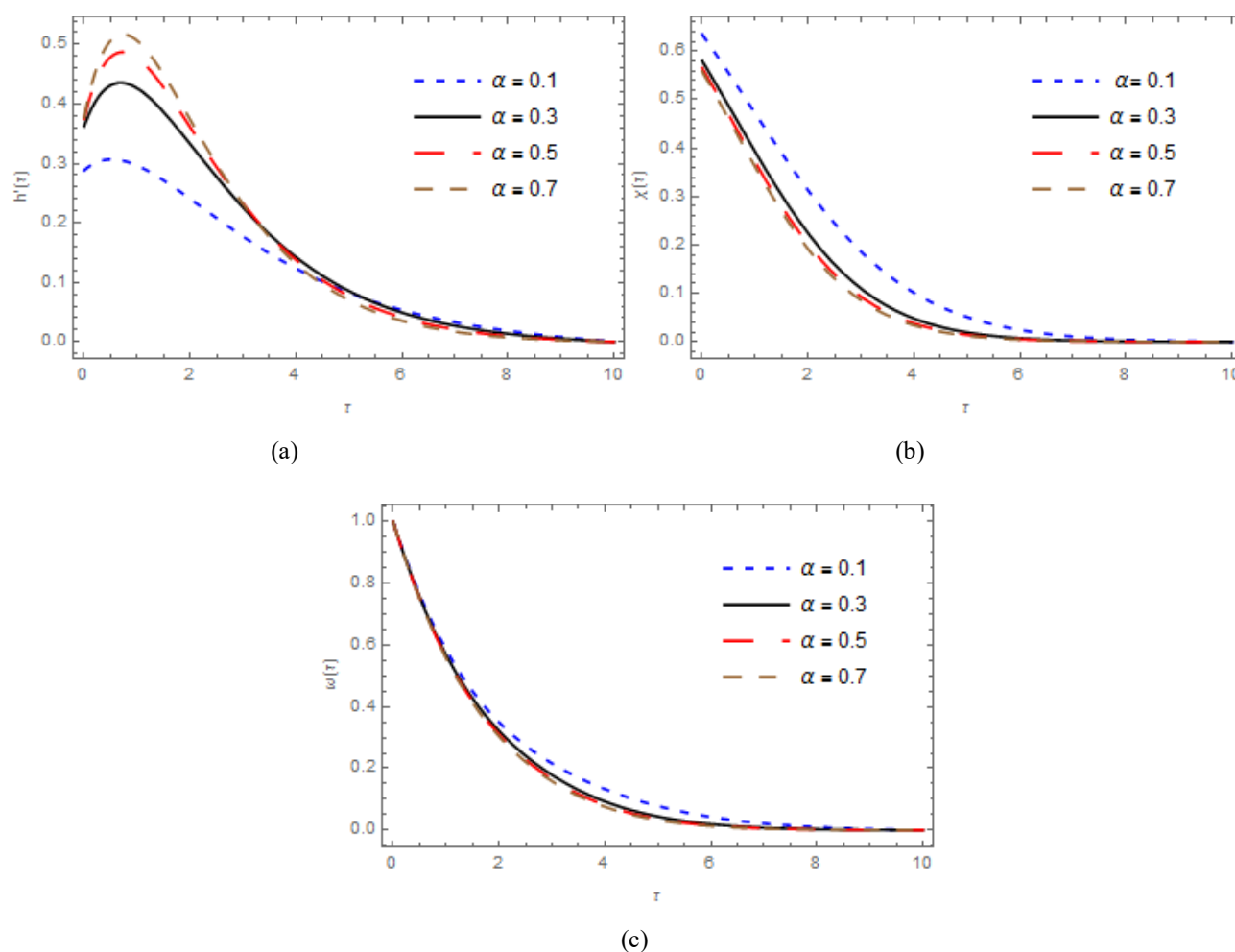


Fig. 7. Casson parameter (α) impact on (a) velocity, (b) temperature, and (c) concentration fields

Figure 7 (a, b, and c) project the impact of Casson parameter (α) on velocity, temperature, and concentration profiles respectively. It is shown from the figures that a hike in the Casson parameter speeds up the velocity distribution and slows down the temperature and nanoparticle volume fraction distribution. Physically, Casson fluid exhibits a solid characteristic when yield stress is more than the shear stress, on the other hand, it behaves as fluid under a reverse trend.

Figure 8(a and b) gives the effects of slip (s_2) on velocity and temperature distributions. It is clearly seen that the velocity raises with the slip impact, while temperature reduces with an increase in the slip parameter. In reality, whenever the slip parameter increases, the fluid particles keep their distance from the plate which leads to a reduction in shear force and accelerates fluid velocity accordingly.

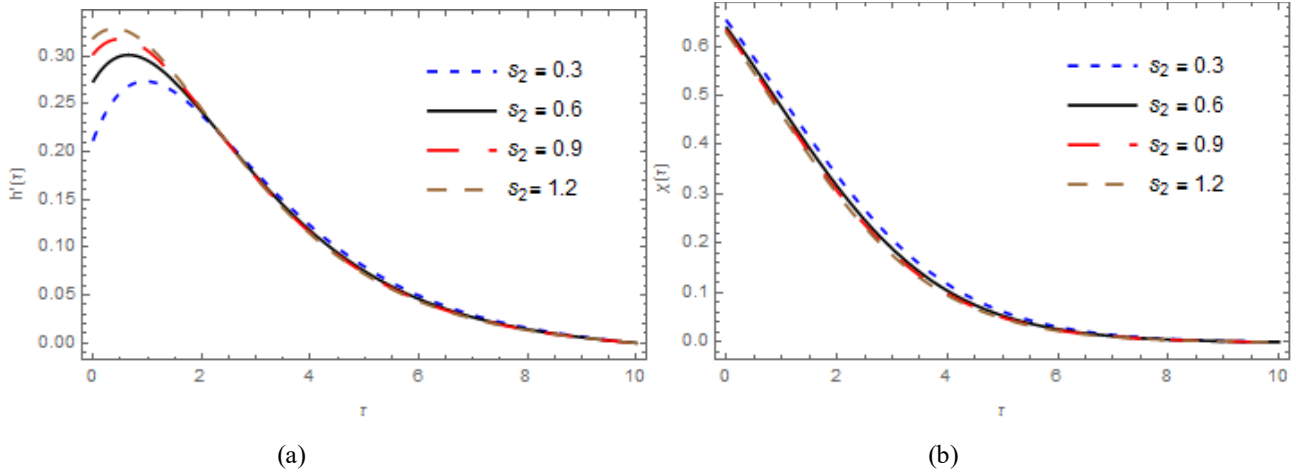


Fig. 8. Velocity slip (S_2) impact on (a) velocity, and (b) temperature fields

5. Conclusions

This study analyzed the influence of variable properties on the quadratic convective flow of Casson nanofluid past an inclined plane. The nonlinearities convention considered in buoyancy force due to heat transfer properties and the notable physical significance of the fluid flow is applicable in industries, most especially in the area of combustion, electronic cooling, reactor safety, thermal systems among others, which demonstrates its phenomenon in the process of heat and mass transfer. The governing model equations are non-dimensionalized and transformed via a suitable similarity transformation to nonlinear ordinary systems of equations. Using the collocation method base on the Legendre polynomial basis function, the resulting systems of ODEs were solved numerically. The impact of various pertinent parameters of interest involved in the problem was observed and clarified through tables and graphs. From the study, the following conclusions are drawn.

1. The velocity is appreciated with α , γ_2 , ε_1 , ε_2 and depreciated with a rise in γ_1 and δ .
2. The energy profiles improved with $\gamma_1, \gamma_2, \delta$ and declined with an increase in ε_1 , α , and S_2 .
3. The nanoparticle volume fraction profiles are elevated with δ and depressed with a hike in γ_2 and α .
4. The rate of heat transfer appreciated with ε_2 and depreciated with higher values of γ_1 , ε_1 and γ_2 .
5. The rate of mass transfer speeds up with γ_2 , ε_2 and slow down with a raise in γ_1 and ε_1 .

Nomenclature

κ	thermal conductivity
k_p	porous medium permeability
g	acceleration due to gravity

D_T	thermophoresis coefficient
D_B	mass diffusion coefficient
c_s	absorption susceptibility
D_m	Brownian coefficient
c_p	specific heat capacity
$h_f(\bar{y}_1)$	heat transfer coefficient
ρ_f	fluid density
τ	ratios of the nanoparticle to base fluid heat capacity
k_1	absorption constants
Q_1	dimensional internal heat generation
λ_1	linear thermal expansion coefficient
λ_3	linear solutal expansion coefficient
\bar{u}_1, \bar{u}_2	Fluid velocities along \bar{y}_1 , \bar{y}_2 respectively
a_j	variation of thermal conductivity
G	heat source parameter
Nb	Brownian motion
Pr	Prandtl number
Nt	thermophoresis parameter
Ra	Rayleigh number
Le	Lewis number
Df	diffusion-thermo parameter
Da	Darcy number
ρ_p	density of nanoparticle
T_m	Fluid temperature
μ	constant coefficient of viscosity
k_0	thermal-diffusion ratio
k^*	constant rate of chemical reaction

b^*	Forchheimer's initial coefficient
ρ_p	density of nanofluid
B_0	constant magnetic field
σ_0	constant electric conductivity
β_0	volumetric thermal expansion
α	Casson parameter
σ_1	Stefan-Boltzmann Rossland
δ	Inclination angle
λ_2	nonlinear convection parameter due to temperature
λ_4	nonlinear convection parameter due to concentration
s_1	Slip parameter
a_i	variation of viscosity
J	magnetic field parameter
γ	chemical reaction parameter
Ec	Eckert number
Nr	buoyancy ratio
Sr	thermal-diffusion parameter
R	radiation parameter
B	Forchheimer parameter
Bi	Biot number

References

- Akolade, M.T., Idowu, A.S., Adeosun, A.T., (2021a). Multislip and Soret–Dufour influence on nonlinear convection flow of MHD dissipative casson fluid over a slendering stretching sheet with generalized heat flux phenomenon. *Heat Trans. Res.*, 50(4): 3913-3933.
- Akolade, M.T., Adeosun, A.T., and Olabode, J.O., (2021b). Influence of thermophysical features on MHD squeezed flow of dissipative Casson fluid with chemical and radiative effects, *J. Appl. Comp. Mech.*, doi: 10.22055/jacm.2020.34909.2508
- Animasaun, I.L., (2015). Effect of thermophoresis, variable viscosity and thermal conductivity on free convective heat and Mass transfer of non-Darcian MHD dissipative casson fluid flow with suction and nth chemical reaction. *J. Nig. Math. Soc.* 34:11-31.
- Asogwa, K.K., Ibe, A.A. and Kenneth, K., (2020). A study of MHD Casson fluid flow over a permeable stretching sheet with Heat and mass transfer. *J. eng. Res. Rep.* 16(2):10-25.
- Gbadeyan, J.A., Titiloye, E.O. and Adeosun, A.T., (2020). Effect of variable thermal conductivity and viscosity on Casson nanofluid flow with convective heating and velocity slip. *Heliyon*, 1(6): e03076.
- Hayat, T., Naz, S., Waqas, M., and Alsaedi, A., (2018). Effectiveness of Darcy-forehhamer and Nonlinear mixed convection aspects in stratified maxwell nanomaterial flow induced by convectively heated surface. *Appl. math. mech. Engli. Ed.*, 39(10):1373-1384.
- Hayat, T., Khan, M.I., Farooq, M., Gull, N. and Alsaedi, A., (2016). Unsteady three-dimensional mixed convection flow with variable viscosity and thermal conductivity. *J. Molecular Liq.*, 223: 1297-1310.
- Ibrahim, S.M., Lorenzini, G., kumar, P.V., and Raju, C.S.K. (2017). Influence of chemical reaction and heat source on dissipative MHD mixed convection flow of a casson nanofluid over a nonlinear permeable stretching sheet. *Int. J. Heat mass transf.* 111: 346-355.
- Idowu, A.S., Akolade, M.T., Abubakar, J.U., and Falodun, B.O., (2020). MHD free convective heat and mass transfer flow of dissipative Casson fluid with variable viscosity and thermal conductivity effects. *J Taibah Uni Sci.*, 14(1):851-862.
- Idowu, A.S., Akolade, M.T., Oyekunle, T.L., and Abubakar, J.U., (2021) Nonlinear convection flow of dissipative Casson nanofluid through an inclined annular microchannel with a porous medium. *Heat Trans. Res.*, 50(4): 3388-3406.
- Idowu, A.S., and Falodun, B.O., (2020) Variable thermal conductivity and viscosity effects on non-Newtonian fluids flow through a vertical porous plate under Soret-Dufour influence. *Math. Comp. Simul.* 177:358-384.
- Jawali, C.U and Chamkha, A.J., (2015). Combined effect of variable viscosity and thermal conductivity on free convection flow of a viscous fluid in a vertical channel. *Int. J Num. meth. Heat flow.* 26(1):18-39.
- Jha, B. K., and Sarki, M. N., (2019). Chemical reaction and Dufour effects on nonlinear free convection heat and mass transfer flow near a vertical moving porous plate. *Heat Trans Res.* 1-16.
- Kala, B.S., Rawat, M.S., and kumar, A., (2020). Numerical Analysis of the flow of a casson fluid in magnetic field over an inclined nonlinear stretching surface with velocity slip in a forchhelmer porous Medium. *Asian J. Math.* 16(7):34-58.
- Kench, J. and Hazarika, G.C., (2017). Effects of variable viscosity and thermal conductivity on hydromagnetic flow of Dusty fluid past a Rotating vertical cone. *Res. J. Eng. Tech.*, 8(1),1-9.
- Kumar, R. and Sood, S. (2016) Interaction of magnetic field and Nonlinear convection in the stagnation point flow over a shrinking sheet. *J. Eng.* [http://dx.doi.org/10.1155/2016/6752520.\(1-8\)](http://dx.doi.org/10.1155/2016/6752520.(1-8))
- Kumar R., Sood, S., Sheikholeslami, M., and Shehzad, S.A (2017a) Nonlinear thermal radiation and cubic autocatalysis chemical reaction effects on the flow of stretched nanofluid under rotational oscillations. *J colloid interface sci.*, 505: 253-265.
- Malik, M.Y., Jamil, H., Salahuddin, T., Bilal, S., Rehman, K.U., and Mustafa, Z., (2016). Mixed convection dissipative viscous fluid flow over a rotating cone by way variable viscosity and thermal conductivity. *Res. Phy.*, 6:1126-1135

- Nagendramma, V., Raju, C.S.K., Mallikarjuna, B., Shehzad, S.A., and Leelarathnam, A. (2018). 3D casson nanofluid flow over slendering surface in a suspension of gyrotactic microorganisms with cattano-christov heat flux. *Appl. Math. Mech.*, 39:623-628.
- Patil P.M and Kulkarni M., (2019). Nonlinear mixed convective nanofluid flow along moving vertical rough plate. *Revista Mexican fisica*. 66(2):135-161.
- Raju A.B, Raju, G.S.S., and Mallikajuna, B. (2017). unsteady quadratic convective flow of a rotating non-Newton fluid over a rotating cone in a porous medium. *Int. J Adv. Res. Comput. Sci.* 8(7) 68-72.
- Raju A.B., Raju, G.S.S., Mallikarjuna, B. and Raju, C.S.K., (2018). Effect of nonlinear convection and variable properties on darcy flow of Non-Newtonian fluid over a rotating cone. *Int. J. Res. Eng. Appl. Manag* 4(2) 586-594.
- Salawu, S.O. and Dada, M.S., (2016) Radioactive heat transfer of variable viscosity and thermal conductivity effect on inclined magnetic field with dissipation in a non-Darey medium. *J. Nig. Math. soc.*, 35(1), (2016) 93-106.
- Uddin M.J., Khan, W.A., and Ismail, A.I., (2012). MHD free convective boundary layer flow of a nanofluid past a flat vertical plate with Newtonian heating boundary condition, *PLoS ONE* 7, e49499
- Umavathi, J.C., Sheremet, M.A., and Mohiuddin, S., (2017). Combined effect of variable viscosity and thermal conductivity on mixed convection flow of a viscous fluid in a vertical channel in the presence of first order chemical reaction. *European J. Mech. B/fluids*, 58: 98-108.
- Upadhya, S.M., Raju, C.S.K., and Saleem, S., (2018a). Nonlinear unsteady convection on micro and manofluids with cattano-christove heat flux. *Result phy.* 9: 779-786.
- Upadhya, S.M., Raju, C.S.K., Saleem, S. and Alderremy, A.A., (2018b). Modified Fourier heat flux an M H D flow over stretched cylinder filled with dust, Graphene and silver nanoparticles. *Results phy.*, 9:1373-1385.

Acknowledgement

The authors are sincerely thankful to the University of Ilorin, Nigeria, for providing an accommodating environment for the this research interest.